Transport properties of a-Si$_{1-x}$C$_x$:H films investigated by the moving photocarrier grating technique

J. A. Schmidt,* M. Hundhausen, and L. Ley

Institut für Technische Physik, Universität Erlangen-Nürnberg, Erwin-Rommel-Strasse 1, D-91058 Erlangen, Germany
(Received 7 April 2000; revised manuscript received 8 August 2000)

The photoconductivity, electron and hole drift mobility, recombination lifetime, and optical properties of hydrogenated amorphous silicon-carbon alloys have been systematically studied as a function of the optical gap. Samples have been prepared by glow-discharge decomposition of silane-methane mixtures with high hydrogen dilution. The methane concentration in the gas phase has been varied between 0 and 66%, obtaining samples with optical gaps between 1.72 and 2.09 eV. Transport parameters have been measured by using the moving photocarrier grating technique. We have found a large decrease in the electron drift mobility with optical gap, especially when small amounts of carbon are incorporated into the silicon matrix. The hole drift mobility is correlated with the Urbach energy, as predicted by the multiple-trapping model. The recombination lifetime shows a maximum for a gap energy close to 1.85 eV, which we assign to competition between a widening of the band tails and an increase in the density of defects acting as recombination centers. We have observed a power-law dependence of the transport parameters on the generation rate. The characteristic power-law exponents are presented as a function of the optical gap.

I. INTRODUCTION

The preparation and characterization of amorphous hydrogenated silicon-carbon alloys (a-Si$_{1-x}$C$_x$:H) are topics of major interest both fundamentally and technologically. For many useful applications such as window layers for solar cells,[1] electroluminescence devices,[2] phototransistors,[3] color sensors,[4] and light-emitting diodes,[5] a material with good and stable electrical properties is needed. Carbon incorporation into a-Si:H leads to an increase in the optical gap, but the drawback is a deterioration of the photoconductivity.[6] Attempts have been made to find deposition conditions leading to improved electrical properties. It has been found that glow-discharge a-Si$_{1-x}$C$_x$:H deposited under high hydrogen dilution exhibits a lower defect density and a higher photoconductivity gain.[7,8] In order to optimize the material a detailed knowledge of the transport parameters, i.e., electron drift mobility (μ_n), hole drift mobility (μ_p), and recombination lifetime (τ_R), is of importance. Up to now most of the studies have dealt with the steady-state photoconductivity (σ_{ph}). A few groups have measured μ_n (Refs. 9–12) and, to our knowledge, only two groups have measured μ_p (Refs. 11 and 12) as a function of the carbon content.

The dependence of μ_n and τ_R on the generation rate (G) provides another important source of information. The steady-state photoconductivity exhibits a characteristic power-law dependence on the generation rate,[13] $\sigma_{ph} \propto G^\gamma$. Similar expressions can be observed for the drift mobility and the lifetime: $\mu_n \propto G^\delta$, $\tau_R \propto G^\kappa$. The Rose factor γ has been measured for amorphous silicon carbide samples as a function of the carbon content (Ref. 14). On the other hand, up to now the characteristic exponents δ and κ have only been reported for pure amorphous silicon.[15]

The moving photocarrier grating (MPG) technique[16,17] allows us to determine μ_n, μ_p, and τ_R individually. In this work we use the MPG method to study the transport parameters of a-Si$_{1-x}$C$_x$:H samples over a wide range of carbon content. We also report the dependence of the transport parameters on the generation rate and the characteristic power-law exponents as a function of the optical gap.

II. EXPERIMENT

The a-Si$_{1-x}$C$_x$:H samples have been deposited by plasma-enhanced chemical vapor deposition (PECVD) of methane/silane mixtures under high hydrogen dilution in a conventional capacitively coupled reactor. We prepared samples under the following deposition conditions: substrate temperature between 220 and 315 °C, chamber pressure between 0.92 and 2.5 mbar, total flow rate [SiH$_4$+CH$_4$+H$_2$] of 40 standard cubic centimeters per minute (sccm), and frequencies of 13 and 50 MHz. The methane concentration in the gas phase, defined as the ratio $x_{gas}=$[CH$_4$]/[SiH$_4$+CH$_4$], was varied in the range $0 \leq x_{gas} < 0.67$. We used a hydrogen dilution ratio [H$_2$]/[SiH$_4$+CH$_4$+H$_2$]$=0.9$. The deposition regime was the so-called ''low power regime'', where there is no direct dissociation of the CH$_4$ molecule. This results in an effective carbon incorporation of about 1/3 of the gas phase concentration.[6]

Conductivity measurements have been performed in the coplanar configuration, with a gap of 1 mm between two graphite electrodes. The absorption coefficient has been measured by transmittance and reflectance for energies larger than the band gap, while we have used photothermal deflection spectroscopy (PDS) in the subgap region. The visible part of the spectrum was used to estimate the optical gap (E_G) by using the Tauc procedure. The Urbach energy (E_U) was obtained from a fitting of the exponential tail in the absorption coefficient spectrum, while we obtained an estimation of the defect density from the absorption coefficient at a fixed energy $E_G - 0.7$ eV.

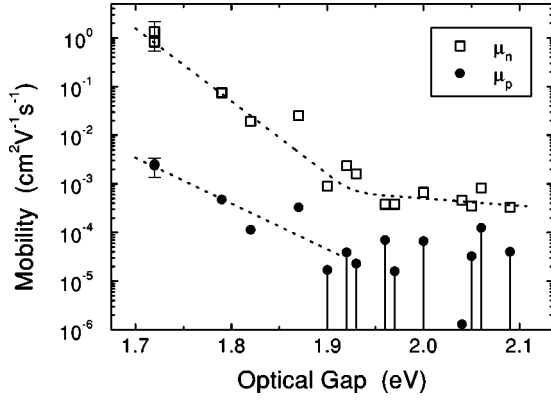In the MPG technique two coherent laser beams are

FIG. 1. Electron and hole drift mobilities as a function of the optical gap E_G. The dotted lines are visual guides. Note that for $E_G \geq 1.9$ eV only upper limits for μ_p are given. Typical error bars are shown.
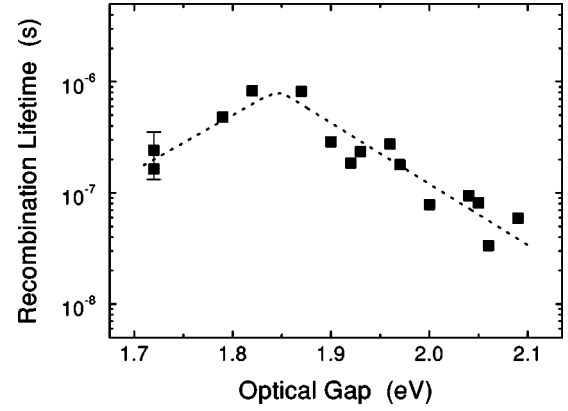

FIG. 2. Recombination lifetime as a function of the optical gap. The dotted line is a visual guide. A typical error bar is shown.

brought to interfere on the surface of the sample. Since a small frequency shift is introduced between the two beams, the resulting interference pattern moves with a velocity $v_{gr} = \lambda \Delta f / [2 \sin(\delta/2)]$, where δ is the angle between the two beams, Δf is the frequency shift, and λ is the laser wavelength. We have used the line $\lambda = 514$ nm from an Ar laser and $\delta = 30°$. Due to their different mobilities, the photogenerated electron and hole distributions have a phase shift. This implies a grating-velocity-dependent dc short circuit current, which allows us to determine independently the photocarrier mobilities and the recombination lifetime.[16,17]

We have applied the MPG technique to a series of 15 samples with optical gaps between 1.72 eV (pure a-Si:H, $x_{gas} = 0$) and 2.09 eV ($x_{gas} = 0.66$). In all cases we have adapted the intensity of the laser beam to get the same generation rate, $G = 8.3 \times 10^{21}$ cm^{-3} s^{-1}. For selected samples with optical gaps of 1.72, 1.82, 1.96, and 2.09 eV we have also measured the dependence of the transport parameters on the generation rate. For each sample we performed about ten MPG measurements in the range 10^{22} cm^{-3} s$^{-1} \geq G \geq 10^{20}$ cm^{-3} s^{-1}, starting from the highest generation rate to avoid subsequent light-induced degradation. We obtained the exponents characterizing the power-law dependence of the transport parameters on the generation rate.

III. RESULTS

In the ''low power'' mode of preparation the carbon sp^3 hybridization of the CH$_4$ precursor is preserved during deposition as methyl groups. Solomon and Tessler[18] have found that in this case the optical gap varies linearly with the carbon content. We find it convenient to present the evolution of the transport parameters as a function of the optical gap, which provides an indirect estimation of the carbon concentration. Samples with the same optical gap have almost the same transport properties, with a secondary influence of the particular deposition conditions. The dependence of the photocarrier mobilities on the optical gap is shown in Fig. 1. As can be seen, the electron drift mobility decreases almost four orders of magnitude when the optical gap increases from 1.72 eV to 2.09 eV. The value obtained for pure amorphous silicon, $\mu_n \approx 1$ cm^2 V^{-1} s^{-1}, is consistent with results from time-of-flight experiments.[19,20] The decrease in μ_n is sharp

until ≈ 1.95 eV, while from this point on there is a saturation around a level $\mu_n \approx 4 \times 10^{-4}$ cm^2 V^{-1} s^{-1}. The hole drift mobility is also influenced by the increase in the carbon content, as also shown in Fig. 1. Note that for $E_G > 1.9$ eV the values given for μ_p are considered as upper limits, since mobilities between zero and the values shown in Fig. 1 provide essentially the same fit to our data. In spite of this fact, our results still show a clear reduction in the hole drift mobility when the optical gap increases.

Figure 2 shows the dependence of the recombination lifetime on the optical gap. We have found that τ_R increases up to $E_G \approx 1.85$ eV and decreases thereafter. As an independent test for the validity of our measurements we have plotted in Fig. 3 a comparison of the mobility-lifetime product obtained from the MPG technique and the steady-state photoconductivity. As can be seen, the values obtained from both methods are in reasonable agreement, mostly within a factor 3, over the whole range of carbon concentrations.

The transport parameters usually depend on the generation rate with a characteristic power-law dependence. The Rose factor γ is defined from the power-law dependence of the steady-state photoconductivity on the generation rate, $\sigma_{ph} \propto G^\gamma$. In a similar fashion we define the parameters δ and κ for the electron drift mobility and the recombination life-
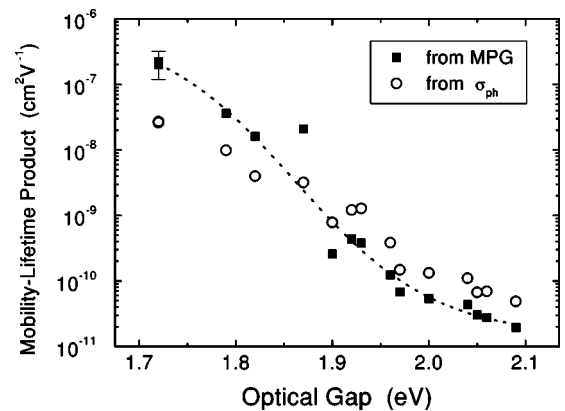

FIG. 3. Mobility-lifetime product as a function of the optical gap. Circles are data obtained from the steady-state photoconductivity, measured with an externally applied voltage of 10 V. Squares are data from the MPG measurements. The dotted line is a visual guide. A typical error bar is shown.
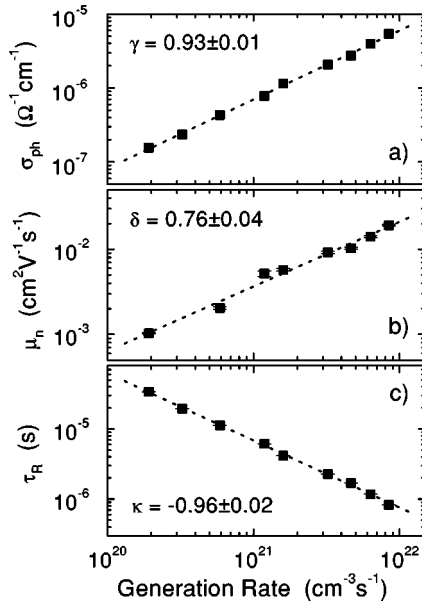
FIG. 4. Evolution of the transport parameters as a function of the generation rate, for a sample with $E_G = 1.82$ eV: (a) steady-state photoconductivity, (b) electron drift mobility, (c) recombination lifetime. The lines are power-law fits; the exponents γ, δ, and κ obtained from the fit are indicated.

time, respectively, according to the expressions $\mu_n \propto G^\delta$ and $\tau_R \propto G^\kappa$. In Fig. 4 we show in a double-logarithmic plot the dependence of σ_{ph}, μ_n, and τ_R on the generation rate. The measurements were taken for a sample with an optical gap of 1.82 eV; for the other samples we observed similar relationships. A linear fit on logarithmic scales allows us to obtain the power-law exponents γ, δ, and κ. In Fig. 5 we show these exponents as a function of the optical gap. The Rose factor γ, shown in Fig. 5(a), increases with E_G in agreement with previous results.[14] The coefficient δ [Fig. 5(b)] also clearly increases with E_G. We have determined $\delta = 0.72$
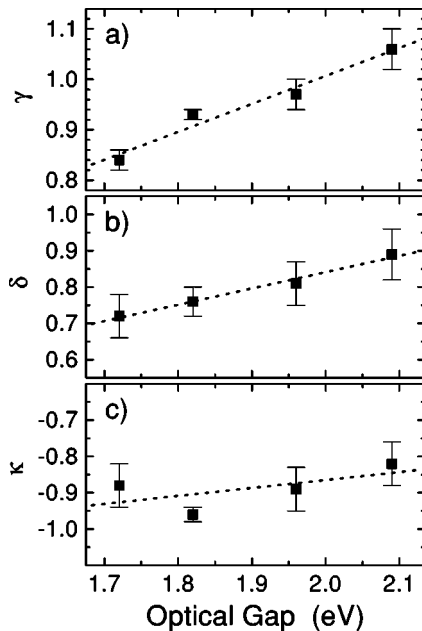

FIG. 5. Evolution of the power-law exponents γ, δ, and κ as a function of the optical gap. The lines are linear fits.
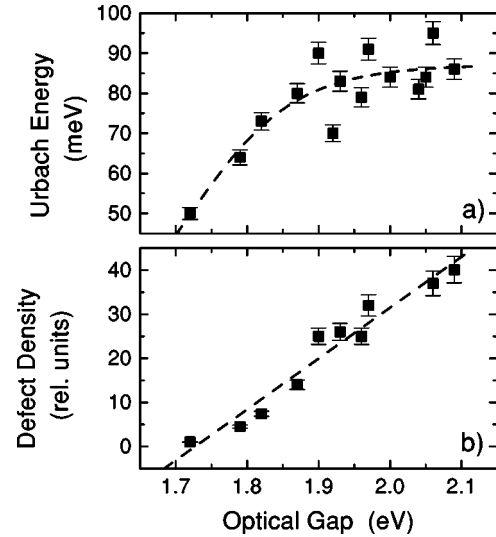

FIG. 6. (a) Urbach energy and (b) defect density as a function of the optical gap. Both parameters are obtained from photothermal deflection spectroscopy. The dotted lines are visual guides. The defect density is given relative to the value for the sample with $E_G = 1.72$ eV.

± 0.06, 0.76 ± 0.04, 0.81 ± 0.06, and 0.89 ± 0.07 for the samples with $E_G = 1.72$, 1.82, 1.96, and 2.09 eV, respectively. From the dependence of the recombination lifetime on the generation rate we have measured $\kappa = -0.88 \pm 0.06$, -0.96 ± 0.02, -0.89 ± 0.06, and -0.82 ± 0.06 for the same set of optical gaps as above. These values are, to our knowledge, the first reports for amorphous hydrogenated silicon-carbon alloys.

IV. DISCUSSION

According to the multiple-trapping model the drift mobility is the free carrier mobility (μ^0) reduced by the fraction of time that the carrier spends in the extended states, so that[21]

$$\mu = \mu^0 \tau_{free} / (\tau_{free} + \tau_{trap}), \qquad (1)$$

where τ_{free} is the free carrier lifetime and τ_{trap} is the time that the carrier spends in band-tail states. The recombination lifetime is the time between excitation and recombination, given by $\tau_R = \tau_{free} + \tau_{trap}$. The incorporation of carbon to the amorphous silicon matrix changes in principle μ^0, τ_{free}, and τ_{trap} simultaneously, so the three parameters can contribute to the decrease of μ_n and μ_p that we observe (see Fig. 1). The free carrier mobility of amorphous materials is limited by the scattering of free carriers due to the intrinsic disorder of the amorphous structure. It is known that carbon incorporation leads to an increase in the amount of structural disorder.[6] Especially for ''low power'' samples, where carbon incorporates as –CH$_3$ groups, a distortion of the silicon network is expected. According to De Seta et al.,[22] the inclusion of C in the network causes strong fluctuations at the top of the valence band. The Urbach energy, which is primarily proportional to the valence-band tail width, is considered to be an indication of the degree of structural disorder. As can be seen in Fig. 6(a), our samples show an increase in the Urbach energy from ≈ 50 meV for $E_G = 1.72$ eV to ≈ 90 meV for $E_G = 2.09$ eV. Thus, the free carrier mobility
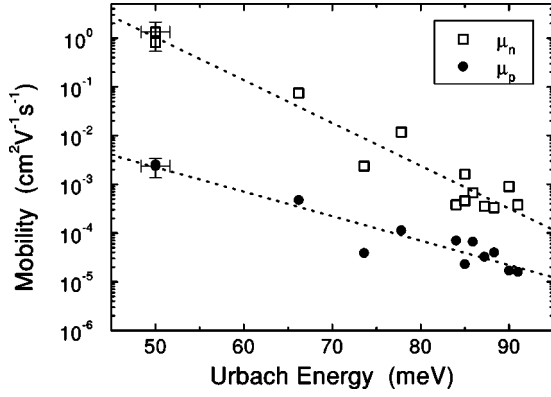
FIG. 7. Correlation between the electron and hole drift mobilities and the Urbach energy. The dotted lines are exponential fits to the measured data. For $E_G > 80$ meV the values for μ_p are the upper limits shown in Fig. 1. Typical error bars are shown.

is expected to decrease with carbon concentration, although the dependence is in principle difficult to quantify.

The free carrier lifetime is determined by[23]

$$\tau_{free} = 1/[N_D \sigma_c v_{th}], \qquad (2)$$

where N_D is the concentration of defects acting as recombination centers, σ_c is its capture cross section, and v_{th} is the thermal velocity of the carriers. In Fig. 6(b) we plot the defect concentration, determined from PDS measurements, as a function of E_G. Assuming that the capture cross sections do not change much with E_G, the increase in the defect density would contribute with a factor of 40 decrease in τ_{free}.

Finally, the time that the carriers spend in shallow band-tail states depends mainly on the energy depth of the states. The increase in the Urbach energy shown in Fig. 6(a) is an indication of a broadening of the valence band tail. The increase is steep until $E_G \approx 1.95$ eV, in agreement with the energy range where the mobility decreases abruptly. This fact points towards a correlation between the hole drift mobility and the Urbach energy. Although less affected by the disorder than the valence-band tail, the conduction-band tail width is also expected to increase with carbon content. Measurements performed by using the time-of-flight transient photoconductivity technique[12] and response time measurements[9] have revealed a widening in the conduction-band tail. The presence of deeper traps increases the reexcitation time of carriers and consequently decreases the drift mobility. Although the Urbach parameter is primarily a measure of the valence-band tail width, a proportionality between valence- and conduction-band tail widths is plausible and theoretically expected.[24] If that is the case, the Urbach parameter would characterize not only the degree of structural disorder but also the width of both band tails. Under these circumstances, a correlation between the drift mobilities and the Urbach parameter should be expected. We indeed find such a correlation, as shown in Fig. 7.

A decrease in μ_n due to carbon alloying has also been observed by other authors. Measurements performed by the time-of-flight technique over a more limited range of optical gaps are in general agreement with our results (a collection of experimental data from different laboratories can be found in the work of Gu et al., Ref. 11). However, these authors
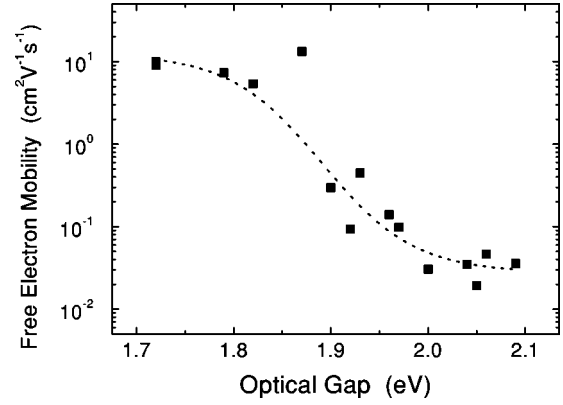

FIG. 8. Free electron mobility as a function of E_G, obtained by introducing in Eq. (3) the data from Figs. 1, 2, and 6(b). The line is a visual guide.

found little change in μ_p with carbon content. Although a correlation between the hole drift mobility and the valence-band tail width is predicted by the multiple-trapping model,[25] Gu et al.[11] did not observe such a correlation, and they argue that the transport mechanism may be more complex than simple multiple trapping, or that the band tails may not be exponential. On the other hand, if we plot μ_p as a function of the Urbach energy, we do see the correlation predicted by the multiple-trapping model, as shown in Fig. 7. Thus, the multiple-trapping model seems to be valid for our samples. The disagreement with the results of Gu et al.[11] may be due to differences in the deposition conditions of the samples.

The dependence of τ_R on E_G shown in Fig. 2 can be explained as the contribution of two factors. On the one hand, the density of midgap states that act as recombination centers increases with carbon content. We have observed this fact in our PDS measurements as a steady increase in the subgap absorption coefficient when E_G increases [Fig. 6(b)]. That effect, which persists in the whole range of optical gaps, tends to shorten the carrier lifetime. On the other hand, we have found a sharp increase in the valence-band tail width when small amounts of carbon are added to the silicon matrix, while further carbon incorporation has a less pronounced effect. An increase in the conduction- and valence-band widths leads to the presence of deeper electron and hole traps. The resulting increase in the reexcitation time may explain the initial increase of the recombination lifetime. When this effect comes to a saturation and the tail width no longer increases, the increase in the density of recombination centers prevails, explaining the decreasing tendency of the lifetime for $E_G > 1.85$ eV.

Knowing the individual dependence of μ_n, τ_{free}, and τ_R as a function of E_G, we are also able to estimate the dependence of the free electron mobility μ_n^0 on E_G. Combining Eqs. (1) and (2) we get

$$\mu_n^0 = \mu_n \tau_R [N_D \sigma_c v_{th}]. \qquad (3)$$

We have assumed the same capture cross section for all the samples, $\sigma_c = 10^{-15}$ cm^2, and $v_{th} = 10^7$ cm/s. These values give $\mu_n^0 = 10$ cm^2 V^{-1} s^{-1} for pure amorphous silicon. By introducing in Eq. (3) μ_n from Fig. 1, τ_R from Fig. 2, and N_D from Fig. 6(b) we obtain the dependence of μ_n^0 on E_G shown in Fig. 8.

We turn now to the discussion of the dependence of the power-law exponents on E_G. According to the results of Fig. 5(a), $\gamma > 1$ for the sample with $E_G = 2.09$ eV. This result has been attributed to the presence of sensitizing states in the valence-band tail, which have a small capture cross section for electrons.[14] When the generation rate increases, the quasi-Fermi-level for holes approaches the valence-band edge, populating these states with holes. The lower capture cross section for electrons implies that holes in these states have a longer lifetime (''safe hole traps''). Since electrons recombine with holes, the electron lifetime also increases with the generation rate. The generation-rate-induced quasi-Fermi-level shift is also the reason for the sign of δ and κ. When the quasi-Fermi-levels move towards the band edges there is a decrease in the density of states acting as electron traps and an increase in the density of recombination centers. This implies an increase of the electron drift mobility and a decrease of the recombination lifetime with the generation rate, i.e., $\delta > 0$ and $\kappa < 0$.

The increase of δ with E_G shown in Fig. 5(b) can also be explained qualitatively with simple arguments. As we have mentioned, there is a broadening of the conduction-band tail when the carbon content increases. A wider band tail implies a larger shift of the electron quasi-Fermi-level for a certain variation of the generation rate and consequently a larger δ coefficient. The κ coefficient does not vary significantly with E_G; the values that we have measured for the four samples are all located within $\kappa = -0.89 \pm 0.07$. However, this value itself may seem relatively large. It implies that the total density of electrons (free plus trapped), given by $n_{tot} = G \tau_R$, depends only weakly on G: $n_{tot} \propto G^{0.11}$. On the other hand the free electron density, proportional to σ_{ph}, evolves as $n_{free} \propto G^\gamma$ with $\gamma \approx 0.88$. It should be noted, however, that for the generation rates typically used in our experiments, most of the charge resides in localized states. In order to visualize the distribution of charge as a function of the generation rate we performed some computer simulations. We used a standard model[26] based on Shockley-Read statistics and a density of states distribution approximated by parabolic bands, exponential band tails, and correlated defects distributed with a Gaussian profile. The parameters used in our modeling are taken from Ref. 26 and are typical for a-Si:H. In Fig. 9 we present the computed concentrations N_D^0 of neutral dangling bonds, N_D^+ and N_D^- of charged dangling bonds, Q_{cb}^- and Q_{vb}^+ of electrons and holes trapped in conduction- and valence-band-tail states, and n_{free} and p_{free} of free electrons and holes, plotted as a function of the generation rate. The simulations can reproduce quite well the dependence of the transport parameters on the generation rate (see Fig. 10). In the range of generation rates that we have used in our experiments (10^{20} cm^{-3} s$^{-1} < G < 10^{22}$ cm^{-3} s^{-1}) electrons are mainly located in D^- states, while holes are mainly trapped in the conduction-band tail. As can be seen in Fig. 9, N_D^- increases slightly with G, giving rise to the dependence $n_{tot} \propto G^{0.11}$. On the other hand, the density of free electrons increases sharply as $G^{0.88}$. Thus, the computer simulations support our measurements and also give $\kappa \approx -0.89$. The power-law exponent κ has been measured for a-Si:H by Haridim, Zelikson, and Weiser[15] by using small signal transient photoconductivity and the steady-
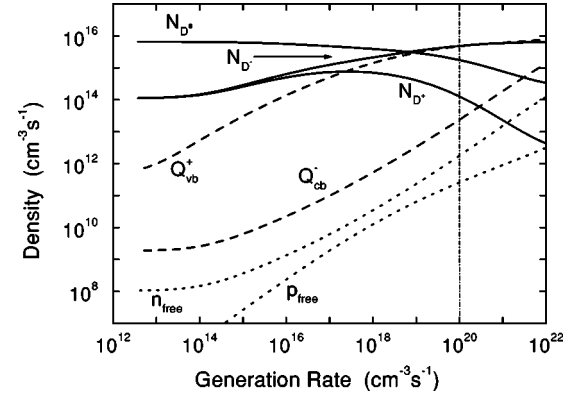
FIG. 9. Computed concentrations N_D^0, N_D^-, and N_D^+ of single, doubly, and unoccupied dangling bonds, respectively, Q_{cb}^- and Q_{vb}^+ of electrons and holes trapped in conduction- and valence-band-tail states, respectively, and n and p of free electrons and holes, as a function of the generation rate. The vertical line indicates the range of values where our measurements were performed ($10^{20} \leqslant G \leqslant 10^{22}$ cm^{-3} s^{-1}).

state photocarrier grating (SSPG) method. From transient photoconductivity they obtained $\kappa \approx -0.73$, while from SSPG they obtained $\kappa \approx -0.96$. Our result for a-Si:H, $\kappa \approx -0.88 \pm 0.06$, is in agreement with their results. It is interesting to note that our results of Fig. 5 show the dependence of the power-law exponents δ and κ as a function of the optical gap.

V. CONCLUSION

We have studied the transport parameters of a-Si$_{1-x}$C$_x$:H alloys as a function of the optical gap by using the moving photocarrier grating technique. When the Tauc gap of the samples increases from 1.72 to ≈ 1.95 eV due to carbon alloying, we observe a sharp increase in the Urbach energy and a concomitant decrease in the electron and hole drift mobilities. A further increase in the Tauc gap, however, results in little change of E_U, μ_n, and μ_p. This fact points towards a correlation between the drift mobilities and E_U. The recombination lifetime shows a maximum for samples with a gap around 1.85 eV. The widening of the band tails,
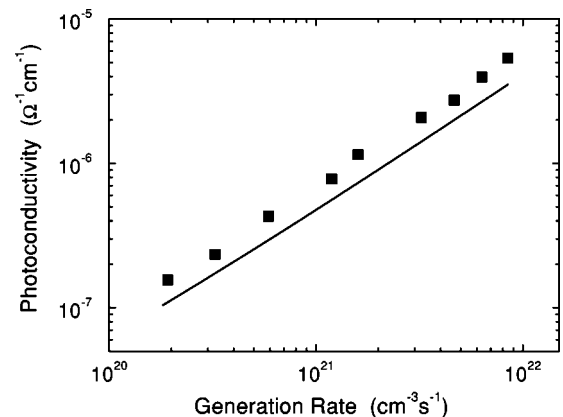
FIG. 10. Photoconductivity as a function of the generation rate. The solid line, obtained from the simulations of Fig. 9 as $\sigma_{ph} = e[\mu_n^0 n_{free} + \mu_p^0 p_{free}]$, reproduces well the experimental values of Fig. 4(a).

which leads to the presence of deeper traps, contributes with an initial increase in the trapping time. For samples with larger gaps, the increase in the density of recombination centers tends to prevail, leading to a final decrease in the recombination lifetime with E_G. We suggest that the combination of these opposite effects explains the observed maximum in τ_R. For selected samples we have also measured the dependence of the transport parameters on the generation rate. We observe a power-law relationship between photoconductivity, electron drift mobility, and recombination lifetime as a function of the generation rate. We show the dependence of the corresponding power-law exponents on the optical gap.

*Permanent address: INTEC (UNL-CONICET), Güemes 3450, 3000 Santa Fe, Argentina.

[1] Y. Tawada, H. Okamoto, and Y. Hamakawa, Appl. Phys. Lett. **42**, 432 (1983).

[2] Y. Hamakawa, D. Kruangam, T. Toyama, M. Yoshimi, S. Paasche, and H. Okamoto, Optoelectronics **4**, 281 (1989).

[3] C.Y. Chang, B.S. Wu, Y.K. Fang, and R.H. Lee, Appl. Phys. Lett. **47**, 49 (1985).

[4] H.K. Tsai, S.C. Lee, and W.L. Lin, IEEE Electron Device Lett. **EDL-8**, 365 (1987).

[5] T. Futagi, N. Ohtani, M. Katsuno, K. Kawamura, J. Ohta, H. Mimura, and K. Kitamura, J. Non-Cryst. Solids **137-138**, 1271 (1991).

[6] J. Bullot and M.P. Schmidt, Phys. Status Solidi B **143**, 345 (1987).

[7] A. Matsuda and K. Tanaka, J. Non-Cryst. Solids **97&98**, 1367 (1987).

[8] F. Alvarez, M. Sebastiani, F. Pozzilli, P. Fiorini, and F. Evangelisti, J. Appl. Phys. **71**, 267 (1992).

[9] Ö. Öktü, T. Tolunay, G.J. Adriaenssens, S.D. Baranovskii, and W. Lauwerens, Philos. Mag. Lett. **68**, 173 (1993).

[10] Y. Tang and R. Braunstein, Appl. Phys. Lett. **66**, 721 (1994).

[11] Q. Gu, Q. Wang, E.A. Schiff, Y-M. Li, and C.T. Malone, J. Appl. Phys. **76**, 2310 (1994).

[12] P.A. Bayley and J.M. Marshall, Philos. Mag. B **73**, 429 (1996).

[13] A. Rose, *Concepts in Photoconductivity and Allied Problems* (Krieger, Huntington, 1978).

[14] F. Demichelis, G. Crovini, C.F. Pirri, E. Tresso, G. Galloni, R. Rizzoli, C. Summonte, F. Zignani, P. Rava, and A. Madam, Philos. Mag. B **69**, 377 (1994).

[15] M. Haridim, M. Zelikson, and K. Weiser, Phys. Rev. B **49**, 13 394 (1994).

[16] U. Haken, M. Hundhausen, and L. Ley, Phys. Rev. B **51**, 10 579 (1995).

[17] M. Hundhausen, J. Non-Cryst. Solids **198-200**, 146 (1996).

[18] I. Solomon and L. Tessler, in *Amorphous Silicon Technology— 1994*, edited by E.A. Schiff, H. Hack, A. Madan, H. Powell, and A. Matsuda, MRS Symposia Proceedings No. 336 (Materials Research Society, Pittsburgh, 1994), p. 505.

[19] J.M. Marshall, R.A. Street, and M.J. Thompson, Phys. Rev. B **29**, 2331 (1984).

[20] A.C. Hourd and W.E. Spear, Philos. Mag. B **51**, L13 (1985).

[21] R.A. Street, *Hydrogenated Amorphous Silicon* (Cambridge University Press, Cambridge, 1991), p. 73.

[22] M. De Seta, S.L. Wang, P. Narducci, and F. Evangelisti, J. Non-Cryst. Solids **137&138**, 851 (1991).

[23] R.A. Street, Ref. 21, p. 311.

[24] Y. Bar-Yam, D. Adler, and J.D. Joannopoulos, Phys. Rev. Lett. **57**, 467 (1986).

[25] T. Tiedje, in *Hydrogenated Amorphous Silicon II*, edited by J.D. Joannopoulos and G. Lucovsky (Springer, New York, 1984), pp. 261–300.

[26] J. Kocka, C.E. Nebel, and C.D. Abel, Philos. Mag. B **63**, 221 (1991).